Available online at www.CivileJournal.org

Civil Engineering Journal

(E-ISSN: 2476-3055; ISSN: 2676-6957)

Vol. 8, No. 01, January, 2022

Exact Three-Dimensional Stability Analysis of Plate Using a Direct Variational Energy Method

F. C. Onyeka [1], B. O. Mama [2], T. E. Okeke [2*]

[1] *Department of Civil Engineering, Edo State University, Uzairue, Edo State, Nigeria.*

[2] *Department of Civil Engineering, University of Nigeria, Nsukka, Nigeria.*

Received 14 September 2021; Revised 16 November 2021; Accepted 11 December 2021; Published 01 January 2022

Abstract

In this paper, direct variational calculus was put into practical use to analyses the three dimensional (3D) stability of rectangular thick plate which was simply supported at all the four edges (SSSS) under uniformly distributed compressive load. In the analysis, both trigonometric and polynomial displacement functions were used. This was done by formulating the equation of total potential energy for a thick plate using the 3D constitutive relations, from then on, the equation of compatibility was obtained to determine the relationship between the rotations and deflection. In the same way, governing equation was obtained through minimization of the total potential energy functional with respect to deflection. The solution of the governing equation is the function for deflection. Functions for rotations were obtained from deflection function using the solution of compatibility equations. These functions, deflection and rotations were substituted back into the energy functional, from where, through minimizations with respect to displacement coefficients, formulas for analysis were obtained. In the result, the critical buckling loads from the present study are higher than those of refined plate theories with 7.70%, signifying the coarseness of the refined plate theories. This amount of difference cannot be overlooked. However, it is shown that, all the recorded average percentage differences between trigonometric and polynomial approaches used in this work and those of 3D exact elasticity theory is lower than 1.0%, confirming the exactness of the present theory. Thus, the exact 3D plate theory obtained, provides a good solution for the stability analysis of plate and, can be recommended for analysis of any type of rectangular plates under the same loading and boundary condition.

Keywords: Exact Solution; Direct Variational Method; Compatibility Governing Equation; Critical Buckling Load; Stability Analysis; Trigonometric; Polynomial Displacement Functions.

1. Introduction

The captivating properties; light weight, economy, and ability to withstand loads, etc. of plate materials have made them to be widely used in different engineering field [1]. Plate structures are used in structural engineering, mechanical engineering, and aerospace engineering etc., in making retaining walls, floor slabs, bridges, railways, ships etc. [2, 3]. The plates are usually under the action of axially compressive or tensile loads acting in the mid-plane of the plate. This axial load at the boundary perpendicular to the mid-surface and distributed through the plate's thickness is known as the in-plane compressive load [4]. The in-plane loading in an elastic plate material beyond its critical values generates structural instability thereby result to the buckling of the plate when a very large stresses are induced [5].

* Corresponding author: edozie.okeke@unn.edu.ng

http://dx.doi.org/10.28991/CEJ-2022-08-01-05

Critical buckling load becomes the greatest load which causes an axially loaded plate to lose its stability [6]. To avoid failure of the plate due to buckling of the plate structure, relatively more accurate and practical studies on stability analysis of plate is required.

The classical plate theory (CPT) based on Kirchhoff assumptions [7] is normally used for plate analysis. The CPT neglects the effect of shear deformation, which would cause the plate to deform thereby making the theory inconsistent. In other words, the thin plate model still makes the assumption that normal stress and strain along the z axis (ε_z and σ_y) are zero and also assumed that the transverse shear stress (τ_{xz} and τ_{yz}) are zero. This assumption has discovered to have introduced errors, hence does not offer a very accurate analysis of plates in which the thickness-to-length proportion is relatively large [8]. Consequently, the refined plate theory (RPT) evolved. The RPT considered the effect of shear deformation. The theory is based on the assumption that the vertical line which is normal to the mid- surface before deformation do not remain normal after deformation, but remain straight [9-11]. The RPT includes; first order shear deformation theory (FSDT or Mindlin plate theory require a shear correction factor in the kinematics formulation to satisfy constitutive relations and achieve accepted variation of transverse shear stress through the thickness of the plate [12-14].

Sadrnejad et al. (2009) and Ghugal et al. (2011) applied the hyperbolic shape function in their work, to obtain the bending and vibration equations of thick rectangular plates while Shufrin (2005) studied the buckling and vibration analysis of thick rectangular plate. Both Sadrnejad et al. (2009), Ghugal et al. (2011) and Sadrnejad et al. (2009) and Sayyad et al. (2012) used FSDT in their analysis, but not considered a polynomial displacement function which is easier to apply or trigonometric function that yields almost an exact function. The FSDT has a limitation of inclusion of a shear correction factor. In avoiding shear correction factor for an improved reliability in the thick plate analysis, a higher order shear deformation theory (HSDT) were implored [12-16]. This is because, the complication (shear correction factor) added produces a limitation when used for the analysis plate especially when the plate is relatively thick. Saffron, and M. Eisenberger (2005) [14] used both first order shear deformation theory (FSDT) and higher order shear deformation theory (HSDT) in their analysis of isotropic plate while Reissner (1979) [15] applied the same to anisotropic plate material. Onyeka et al. (2021) and Senjanović et al. (2013) [17, 18] utilized the analytical approach to get the exact polynomial displacement function from the governing equation. They did not apply trigonometric function which gives closer form solution than polynomial whose exact function tends to infinity. Meanwhile, Reissner (1979), Ibearugbulem (2016), Onyeka et al. (2021) and Senjanović et al. (2013) [15-18] did not consider the effect of the in-plane load on the stability of the structure. The HSDT or moderately thick plate theory developed by previous scholars is an improvement of the FSDT, due to its avoidance of shear correction factor and has been applied successfully by different researchers in the stability analysis of thick plates [19-25].

Reddy and Phan (1985) [19] studied the stability and vibration of isotropic, orthotropic and laminated plates. They applied the higher-order shear deformation theory to obtain the governing equation for the buckling analysis of thick rectangular plate. They also performed the vibration analysis for both isotropic and orthotropic plates, while Ghugal and Sayaad (2014) [20] studied the buckling and vibration of plates using exponential shear deformation theory (ESDT). Sayyad and Ghugal (2012) [21] used the same theory to analyze thick isotropic plates under biaxial and uniaxial in-plane loads using an assumed exponential displacement function. Another study was carried out by Gunjal et al. (2015) [22] using refined trigonometric theory (TSDT) to obtain the buckling load of thick isotropic rectangular plates. Ibearugbulem et al. (2020) [23] used orthogonal polynomial displacement functions (OPDF) and a polynomial shear deformation function f (z) in the buckling analysis of isotropic thick rectangular plate subjected to uniaxial in-plane compressive loading, Nx. The same type of function (polynomial displacement shape function) was also applied by Ezeh et al. (2018) [24], in their work, the free vibration and stability analysis of thick isotropic and orthotropic plates with SSSS and SSFS support conditions were performed by applying the alternative II theory. An alternate II theory is an improved shear deformation theory whose kinematics formulation involves the addition of the classical and shear deformation parts of the in-plane displacements to give the total in-plane displacements. This theory is an improvement on HSDT and FSDT. Meanwhile, literature proves that the formulated Alternative II relationship introduces some error in the result of the analysis [25]. The Alternate I theory formulation circumvents the inclusion of classical plate theory part of the in-plane displacement in the formulation of the total in-plane displacement kinematics. This Alternative I theory is derived from Mindlin theory (without shear correction factor) which is discovered to be an improvement of the Alternative II theory in the thick plate analysis since it proved to be more consistent than other plate theories, but it still poses a limitation of zero vertical stress (σ_z) and strain (ε_z).

Literatures found that previous scholars have studied the stability analysis of plate using CPT and different incomplete 2D theories (including Alternative I and II theory) to determine the buckling load. This makes it an incomplete 3D analytical approach because it does not include all the stress and strain in the plate, rather it neglect the strain and stress along the thickness direction (ε_z and σ_z). It was discovered that neglect of this stress under-estimates the buckling load of the plate, therefore, for a thick plate stability analysis, a typical 3-D analytical plate theory is required. A typical 3-D plate theory involves all the six strains and stress components, unlike RPT and improved RPT which assumed that the strain normal to the x-y plane (σ_z) is so small that it can be neglected Furthermore, it is recorded that previous theories of incomplete 3-D are approximations of the elasticity three-dimensional equilibrium

equations and cannot be reliable for thick plate analysis as they will not give an exact solution. The exact 3-D plate theory gives a value of deflection and buckling load for all the categories of plate (thin, moderately thick and thick plate).

However, Pagano (1970) and Uymaz et al. (2012) studied an exact elastic behavior of bi-directional functionally graded composite plates subjected to different axial loading plates using 3-D plate theory to determine the stress element that induces deformation in the plate structure by employing a the Ritz method with Chebyshev polynomials as assumed displacement functions. Uymaz et al. (2012) considered in-plane load the effect of the in-plane load on the buckling of the plate structure but Pagano (1970) did not consider the effect of the in-plane load on the stability of the structure thereby limited their work. Singh and Singh (2016) solve the same problem using a numerical approach which is an approximate method in the plate analysis. It was discovered that by assuming the displacement function, the result of the 3-D plate stability analysis will also yield an approximate solution [26-29]. An approximate solution is limited in application as it could only give the values of stresses and displacement at a specific point (not any point) of the plate. Lee (1967) [29] overcome that limitation by presenting a 3-D stability analysis of plate using Levy type solution approach derive the governing equation and determine the effect of the in-plane load on the buckling of the plate structure. The Levy being an analytical approach is reliable but poses a challenge of difficulty in solving of Fourier series expansion and the state-space process which is associated to Levy type solution especially when applied in a complex system. Moslemi et al. (2016) [30] studied a 3-D TSDT for rectangular isotropic thick plate analysis, which is simply supported edge. Though the method they applied bridged the limitation associated with the work of Pagano (1970), Uymaz et al. (2012) and Lee (1967) by formulating the exact displacement function, it can be seen in their analysis that they did not apply polynomial function which is easier to apply especially in the case of complex support conditions. They carried out the 3-D stability analysis but they did not obtain the buckling load of simply supported plate by varying stiffness properties and the aspect ratio. This gap in the literature is worth filling.

In this research, an improved three-dimensional elasticity theory was applied in the three-dimensional plate analysis under uniaxial compressive uniformly distributed load. The aim of this work is to study the exact three-dimensional stability analysis of rectangular plates that is simply supported at the four edges to determine the critical buckling load using the variational method.

2. Research Methodology

In this section, the formulation and derivation of the equations for the analysis in this study are achieved. Different stages of the processes involved in achieving the goal are presented in the flowchart. The shows the procedures taken in the determination of the critical buckling load for the three- dimensional stability analysis of thick plate.

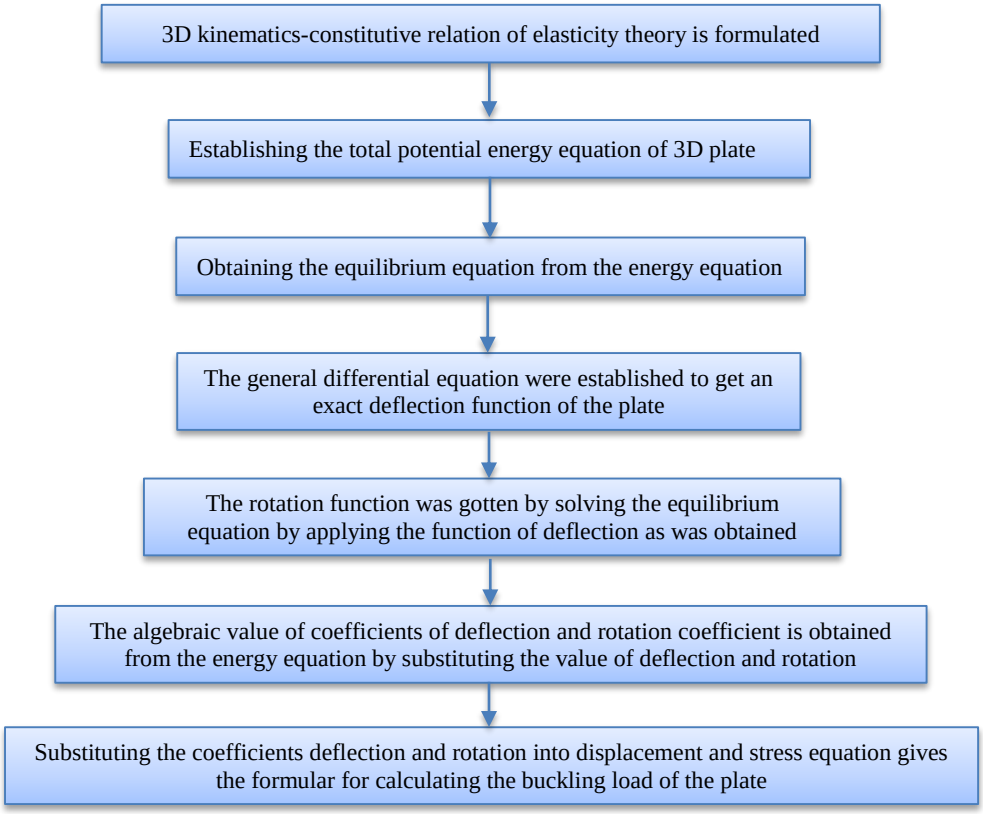

Figure 1. Flowchart of the research methodology

2.1. Kinematics

The displacement field includes the displacements along x, y and z-axes: u, v and w respectively. After bending of the plate the x-z section and y-z section, which are initially normal to the x-y plane before bending go off normal to the x-y plane as seen in Figure 2. Six strain components are:

$$\varepsilon_x = \frac{\partial u}{dx} = z\frac{\partial \theta_x}{\partial x} \quad (1)$$

$$\varepsilon_y = \frac{\partial v}{\partial y} = z\frac{\partial \theta_y}{\partial y} \quad (2)$$

$$\varepsilon_z = \frac{\partial w}{\partial z} \quad (3)$$

$$\gamma_{xy} = \frac{\partial u}{\partial y} + \frac{\partial v}{\partial x} = z\frac{\partial \theta_x}{\partial y} + z\frac{\partial \theta_y}{\partial x} \quad (4)$$

$$\gamma_{xz} = \frac{\partial u}{\partial z} + \frac{\partial w}{\partial x} = \theta_x + \frac{\partial w}{\partial x} \quad (5)$$

$$\gamma_{yz} = \frac{\partial v}{\partial z} + \frac{\partial w}{\partial y} = \theta_y + \frac{\partial w}{\partial y} \quad (6)$$

Where; The symbol w denotes deflection, the symbol u denotes in-plane displacement along x-axis, the symbol v denotes in-plane displacement along y-axis, the symbol θ_x denotes shear deformation rotation along x axis, the symbol θ_y denotes shear deformation rotation along the y axis, the symbol ε_x denotes normal strain along x axis, the symbol ε_y denotes normal strain along y axis, the symbol ε_z denotes normal strain along z axis, the symbol γ_{xy} denotes shear strain in the plane parallel to the x-y plane, the symbol γ_{xz} denotes shear strain in the plane parallel to the x-z plane, the symbol γ_{yz} denotes shear strain in the plane parallel to the y-z plane.

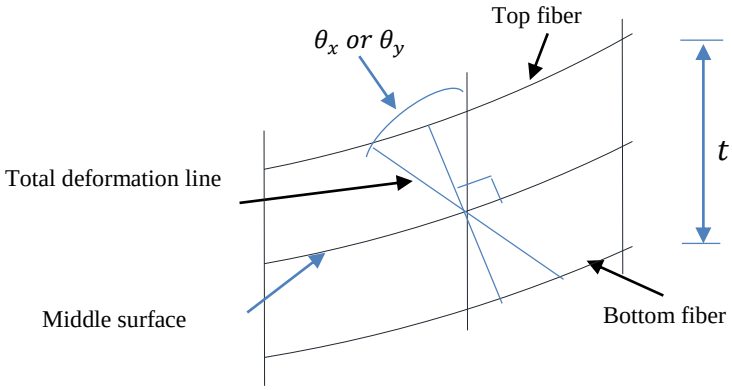

Figure 2. Rotation of x-z (or y-z) section after bending

The spatial dimensions of the plate along x, y and z-axes are a, b and t respectively. More so, the non-dimensional form of coordinates are R = x/a, Q = y/b and S = z/t corresponding to x, y and z-axes respectively. The aspect ratio (b/a) is denoted as β. In terms of non-dimensional coordinates the six strain components are written as:

$$\varepsilon_x = \frac{St}{a}\frac{\partial \theta_x}{\partial R} \quad (7)$$

$$\varepsilon_y = \frac{St}{a\beta}\frac{\partial \theta_y}{\partial Q} \quad (8)$$

$$\varepsilon_z = \frac{1}{t}\frac{\partial w}{\partial S} \quad (9)$$

$$\gamma_{xy} = \frac{St}{a\beta}\frac{\partial \theta_x}{\partial Q} + \frac{St}{a}\frac{\partial \theta_y}{\partial R} \quad (10)$$

$$\gamma_{xz} = \theta_x + \frac{1}{a}\frac{\partial w}{\partial R} \quad (11)$$

$$\gamma_{yz} = \theta_y + \frac{1}{a\beta}\frac{\partial w}{\partial Q} \quad (12)$$

2.2. Stress-Strain Relation

The stress-strain relationship are analyzed in this section by applying the established relation (strain-displacement relation) in the previous section, to determine the value of stresses in the plate. These stresses are described using generalized Hooke's law given as:

$$\begin{bmatrix}\sigma_x\\ \sigma_y\\ \sigma_z\\ \gamma_{xz}\\ \gamma_{yz}\\ \gamma_{xy}\end{bmatrix} = \frac{E}{(1+\mu)(1-2\mu)}\begin{bmatrix}(1-\mu) & \mu & \mu & 0 & 0 & 0\\ \mu & (1-\mu) & \mu & 0 & 0 & 0\\ \mu & \mu & (1-\mu) & 0 & 0 & 0\\ 0 & 0 & 0 & \left(\frac{1-2\mu}{2}\right) & 0 & 0\\ 0 & 0 & 0 & 0 & \left(\frac{1-2\mu}{2}\right) & 0\\ 0 & 0 & 0 & 0 & 0 & \left(\frac{1-2\mu}{2}\right)\end{bmatrix}\begin{bmatrix}\varepsilon_x\\ \varepsilon_y\\ \varepsilon_z\\ \gamma_{xz}\\ \gamma_{yz}\\ \gamma_{xy}\end{bmatrix} \quad (13)$$

Substituting Equations 7 to 12 into Equation 13 and writing the equations of the six stress components one by one in term of the displacements gives:

$$\sigma_x = \frac{EtS}{(1+\mu)(1-2\mu)a}\left[(1-\mu).\frac{\partial\theta_x}{\partial R} + \frac{\mu}{\beta}.\frac{\partial\theta_y}{\partial Q} + \frac{\mu a}{St^2}.\frac{\partial w}{\partial S}\right] \quad (14)$$

$$\sigma_y = \frac{EtS}{(1+\mu)(1-2\mu)a}\left[\mu.\frac{\partial\theta_x}{\partial R} + \frac{(1-\mu)}{\beta}.\frac{\partial\theta_y}{\partial Q} + \frac{\mu a}{St^2}.\frac{\partial w}{\partial S}\right] \quad (15)$$

$$\sigma_z = \frac{EtS}{(1+\mu)(1-2\mu)a}\left[\mu.\frac{\partial\theta_x}{\partial R} + \frac{\mu}{\beta}.\frac{\partial\theta_y}{\partial Q} + \frac{(1-\mu)a}{St^2}.\frac{\partial w}{\partial S}\right] \quad (16)$$

$$\tau_{xy} = \frac{E(1-2\mu)tS}{2(1+\mu)(1-2\mu)a}.\left[\frac{1}{\beta}\frac{\partial\theta_x}{\partial Q} + \frac{\partial\theta_y}{\partial R}\right] \quad (17)$$

$$\tau_{xz} = \frac{E(1-2\mu)tS}{2(1+\mu)(1-2\mu)a}.\left[\frac{a}{tS}\theta_x + \frac{1}{tS}\frac{\partial w}{\partial R}\right] \quad (18)$$

$$\tau_{yz} = \frac{E(1-2\mu)tS}{2(1+\mu)(1-2\mu)a}.\left[\frac{a}{tS}\theta_y + \frac{1}{\beta tS}\frac{\partial w}{\partial Q}\right] \quad (19)$$

Where: the symbol μ denotes poisons ratio, the symbol E denotes modulus of elasticity of the plate, the symbol σ_x denotes stress normal along x axis, the symbol σ_y denotes stress normal along the y axis, σ_z denotes stress normal along the z axis, the symbol τ_{xy} denotes shear stress along the x-y axis, the symbol τ_{xz} denotes shear stress along the x-z axis, the symbol τ_{yz} denotes shear stress along the y-z axis.

2.3. Strain Energy

Strain energy is defined as the average of the product of stress and strain over the volume of the plate. This is expressed mathematically as:

$$U = \frac{1}{2}\int_0^a\int_0^b\int_{-0.5t}^{0.5t}\sigma.\varepsilon\,dx\,dy\,dz = \frac{abt}{2}\int_0^1\int_0^1\int_{-0.5}^{0.5}\sigma.\varepsilon\,dR\,dQ\,dS \quad (20)$$

Substituting Equations 7 to 12 and Equations 14 to 19 into Equation 20 gives:

$$U = \frac{Et^3ab}{2(1+\mu)(1-2\mu)a^2}\int_0^1\int_0^1\int_{-0.5}^{0.5}\left[(1-\mu)S^2\left(\frac{\partial\theta_x}{\partial R}\right)^2 + \frac{S^2}{\beta}\frac{\partial\theta_x}{\partial R}.\frac{\partial\theta_y}{\partial Q} + \frac{(1-\mu)}{\beta^2}S^2\left(\frac{\partial\theta_y}{\partial Q}\right)^2 + \frac{(1-2\mu)}{2\beta^2}S^2\left(\frac{\partial\theta_x}{\partial Q}\right)^2 + \frac{(1-2\mu)}{2}S^2\left(\frac{\partial\theta_y}{\partial R}\right)^2 + \frac{(1-2\mu)}{2t^2}\left(a^2{\theta_x}^2 + a^2{\theta_y}^2 + \left(\frac{\partial w}{\partial R}\right)^2 + \frac{S^2}{\beta^2}\left(\frac{\partial w}{\partial Q}\right)^2 + 2a.\theta_x S^2\frac{\partial w}{\partial R} + \frac{2a.\theta_y}{\beta}S^2\frac{\partial w}{\partial Q}\right) + 2S\frac{\mu a}{t^2}.\left(\frac{\partial\theta_x}{\partial R}.\frac{\partial w}{\partial S} + \frac{1}{\beta}.\frac{\partial\theta_y}{\partial Q}.\frac{\partial w}{\partial S}\right) + \frac{(1-\mu)a^2}{t^4}\left(\frac{\partial w}{\partial S}\right)^2\right]dR\,dQ\,dS \quad (21)$$

Simplifying and carrying out the integration of Equation 21 with respect to S gives:

$$U = \frac{D^*ab}{2a^2}\int_0^1\int_0^1\left[(1-\mu)\left(\frac{\partial\theta_x}{\partial R}\right)^2 + \frac{1}{\beta}\frac{\partial\theta_x}{\partial R}.\frac{\partial\theta_y}{\partial Q} + \frac{(1-\mu)}{\beta^2}\left(\frac{\partial\theta_y}{\partial Q}\right)^2 + \frac{(1-2\mu)}{2\beta^2}\left(\frac{\partial\theta_x}{\partial Q}\right)^2 + \frac{(1-2\mu)}{2}\left(\frac{\partial\theta_y}{\partial R}\right)^2 + \frac{6(1-2\mu)}{t^2}\left(a^2{\theta_x}^2 + a^2{\theta_y}^2 + \left(\frac{\partial w}{\partial R}\right)^2 + \frac{1}{\beta^2}\left(\frac{\partial w}{\partial Q}\right)^2 + 2a.\theta_x\frac{\partial w}{\partial R} + \frac{2a.\theta_y}{\beta}\frac{\partial w}{\partial Q}\right) + \frac{(1-\mu)a^2}{t^4}\left(\frac{\partial w}{\partial S}\right)^2\right]dR\,dQ \quad (22)$$

Given that D^* is the Rigidity for three-dimensional thick plate, let:

$$D^* = \frac{Et^3}{12(1+\mu)(1-2\mu)} = D\,\frac{(1-\mu)}{(1-2\mu)} \tag{23}$$

Given that D is the Rigidity of the CPT or incomplete three-dimensional thick plate, let:

$$D = \frac{Et^3}{12(1-\mu^2)} \tag{23b}$$

2.4. Total Potential Energy Functional

The total potential energy function (Π) is the algebraic summation of strain energy (U) and external work (V). That is:

$$\Pi = U - V \tag{24}$$

However, the external work for buckling load is given as:

$$V = \frac{abN_x}{2a^2}\int_0^a \int_0^b \left(\frac{\partial w}{\partial R}\right)^2 dR\, dQ \tag{25}$$

Where; N_x is the uniform applied uniaxial compression load of the plate.

Substituting Equations 22 and 25 into Equation 24 gives:

$$\Pi = \frac{D^*ab}{2a^2}\int_0^1 \int_0^1 \left[(1-\mu)\left(\frac{\partial \theta_x}{\partial R}\right)^2 + \frac{1}{\beta}\frac{\partial \theta_x}{\partial R}.\frac{\partial \theta_y}{\partial Q} + \frac{(1-\mu)}{\beta^2}\left(\frac{\partial \theta_y}{\partial Q}\right)^2 + \frac{(1-2\mu)}{2\beta^2}\left(\frac{\partial \theta_x}{\partial Q}\right)^2 + \frac{(1-2\mu)}{2}\left(\frac{\partial \theta_y}{\partial R}\right)^2 + \frac{6(1-2\mu)}{t^2}\left(a^2{\theta_x}^2 + a^2{\theta_y}^2 + \left(\frac{\partial w}{\partial R}\right)^2 + \frac{1}{\beta^2}\left(\frac{\partial w}{\partial Q}\right)^2 + 2a.\theta_x\frac{\partial w}{\partial R} + \frac{2a.\theta_y}{\beta}\frac{\partial w}{\partial Q}\right) + \frac{(1-\mu)a^2}{t^4}\left(\frac{\partial w}{\partial S}\right)^2 - \frac{N_x}{D^*}.\left(\frac{\partial w}{\partial R}\right)^2\right] dR\, dQ \tag{26}$$

2.5. Compatibility Equation

The minimization of the total potential energy functional with respect to θ_x and θ_y gives the equilibrium equation (Compatibility Equation) to the rotation about the axis x and y as presented in Equation 27 and 28 respectively:

$$\frac{\partial \Pi}{\partial \theta_x} = \frac{D^*ab}{2a^2}\int_0^1 \int_0^1 \left[(1-\mu)\frac{\partial^2 \theta_x}{\partial R^2} + \frac{1}{2\beta}.\frac{\partial^2 \theta_y}{\partial R \partial Q} + \frac{(1-2\mu)}{2\beta^2}\frac{\partial^2 \theta_x}{\partial Q^2} + \frac{6(1-2\mu)}{t^2}\left(a^2\theta_x + a.\frac{\partial w}{\partial R}\right)\right] dR\, dQ = 0 \tag{27}$$

$$\frac{\partial \Pi}{\partial \theta_y} = \frac{D^*ab}{2a^2}\int_0^1 \int_0^1 \left[\frac{1}{2\beta}.\frac{\partial^2 \theta_x}{\partial R \partial Q} + \frac{(1-\mu)}{\beta^2}\frac{\partial^2 \theta_y}{\partial Q^2} + \frac{(1-2\mu)}{2}\frac{\partial^2 \theta_y}{\partial R^2} + \frac{6(1-2\mu)}{t^2}\left(a^2\theta_y + \frac{a.}{\beta}\frac{\partial w}{\partial Q}\right)\right] dR\, dQ = 0 \tag{28}$$

2.6. Solution to Compatibility Equations

The governing equation in this study was solved twice. Firstly, it was solved analytically in this section, to relate one variable to another variable with many unknown coefficients thereby yielding a solution of the compatibility equation as determined in Equation 46. This was done by substituting Equation 46 into Equation 48 (Governing Equation) to get Equation 49. The aim is to use Equation 46 to simplify the complex Equation 48 to yield Equation 49. Secondly, it was solved numerically in the subsequent section to get the exact equation for those unknown coefficients by getting the unknown constant which will yield two governing equations of a 3-dimensional rectangular plate in Equation 57 and 58. The solution of Equation 57 and 58 yields an exact solution to the differential equation for deflection and buckling load (67a, b) and (90 or 91) respectively. The Equation (67a, b) becomes the general characteristic equation which is an expression that when subjected to a particular boundary condition will yield a particular solution for the deflection in Equation (92a, b).

We get general solution that will be from the law of addition, the two terms can be added when they are of the same nature. Using law Equations 11 and 12 can be rewritten as:

$$\theta_x = \gamma_{xz} - \frac{1}{a}.\frac{\partial w}{\partial R} = \frac{c}{a}\frac{\partial w}{\partial R} \tag{29}$$

$$\theta_y = \gamma_{yz} - \frac{1}{a\beta}.\frac{\partial w}{\partial Q} = \frac{c}{a\beta}.\frac{\partial w}{\partial Q} \tag{30}$$

Where c is a quantity whose expression or value shall be obtained later.

For Equation 27 to be true, its integrands can be taken to be zero. That is:

$$(1-\mu)\frac{\partial^2\theta_x}{\partial R^2}+\frac{1}{2\beta}.\frac{\partial^2\theta_y}{\partial R\partial Q}+\frac{(1-2\mu)}{2\beta^2}\frac{\partial^2\theta_x}{\partial Q^2}+\frac{6(1-2\mu)}{t^2}\left(a^2\theta_x+a.\frac{\partial w}{\partial R}\right)=0 \quad (31)$$

For Equation 28 to be true, its integrands can be taken to be zero. That is:

$$\frac{1}{2\beta}.\frac{\partial^2\theta_x}{\partial R\partial Q}+\frac{(1-\mu)}{\beta^2}\frac{\partial^2\theta_y}{\partial Q^2}+\frac{(1-2\mu)}{2}\frac{\partial^2\theta_y}{\partial R^2}+\frac{6(1-2\mu)}{t^2}\left(a^2\theta_y+\frac{a.}{\beta}\frac{\partial w}{\partial Q}\right)=0 \quad (32)$$

Substituting Equation 29 into Equation 31, simplifying and factorizing the outcome gives:

$$\frac{\partial w}{\partial R}\left[(1-\mu)\frac{\partial^2 w}{\partial R^2}+\frac{1}{\beta^2}.\frac{\partial^2 w}{\partial Q^2}(1-\mu)+\frac{6(1-2\mu)a^2}{t^2}.\left(1+\frac{1}{c}\right)\right]=0 \quad (33)$$

Substituting Equation 30 into Equation 32, simplifying and factorizing the outcome gives:

$$\frac{1}{\beta}.\frac{\partial w}{\partial Q}\left[\frac{\partial^2 w}{\partial R^2}(1-\mu)+\frac{(1-\mu)}{\beta^2}\frac{\partial^2 w}{\partial Q^2}+\frac{6(1-2\mu)a^2}{t^2}.\left(1+\frac{1}{c}\right)\right]=0 \quad (34)$$

Factorizing Equation 33 gives:

$$\frac{\partial w}{\partial R}\left[(1-\mu)\frac{\partial^2 w}{\partial R^2}+\frac{1}{2\beta^2}.\frac{\partial^2 w}{\partial Q^2}+\frac{(1-2\mu)}{2\beta^2}\frac{\partial^2 w}{\partial Q^2}+\frac{6(1-2\mu)a^2}{t^2}.\left(1+\frac{1}{c}\right)\right]=0 \quad (35)$$

Factorizing Equation 34 gives:

$$\frac{1}{\beta}.\frac{\partial w}{\partial Q}\left[\frac{1}{2}.\frac{\partial^2 w}{\partial R^2}+\frac{(1-\mu)}{\beta^2}\frac{\partial^2 w}{\partial Q^2}+\frac{(1-2\mu)}{2}\frac{\partial^2 w}{\partial R^2}+\frac{6(1-2\mu)a^2}{t^2}.\left(1+\frac{1}{c}\right)\right]=0 \quad (36)$$

One of the possibilities of Equation 35 to be true is for the terms in the bracket to sum to zero. That is:

$$(1-\mu)\frac{\partial^2 w}{\partial R^2}+\frac{1}{2\beta^2}.\frac{\partial^2 w}{\partial Q^2}+\frac{(1-2\mu)}{2\beta^2}\frac{\partial^2 w}{\partial Q^2}+\frac{6(1-2\mu)a^2}{t^2}.\left(1+\frac{1}{c}\right)=0 \quad (37)$$

Simplifying Equation 37 gives:

$$(1-\mu)\frac{\partial^2 w}{\partial R^2}+\frac{1}{2\beta^2}.\frac{\partial^2 w}{\partial Q^2}\left(1+(1-2\mu)\right)+\frac{6(1-2\mu)a^2}{t^2}.\left(1+\frac{1}{c}\right)=0 \quad (38)$$

This gives:

$$(1-\mu)\frac{\partial^2 w}{\partial R^2}+\frac{1}{\beta^2}.\frac{\partial^2 w}{\partial Q^2}(1-\mu)+\frac{6(1-2\mu)a^2}{t^2}.\left(1+\frac{1}{c}\right)=0 \quad (39)$$

One of the possibilities of Equation 38 to be true is for the terms in the bracket to sum to zero. That is:

$$\frac{1}{2}.\frac{\partial^2 w}{\partial R^2}+\frac{(1-\mu)}{\beta^2}\frac{\partial^2 w}{\partial Q^2}+\frac{(1-2\mu)}{2}\frac{\partial^2 w}{\partial R^2}+\frac{6(1-2\mu)a^2}{t^2}.\left(1+\frac{1}{c}\right)=0 \quad (40)$$

Simplifying Equation 40 gives:

$$\frac{1}{2}.\frac{\partial^2 w}{\partial R^2}\left(1+(1-2\mu)\right)+\frac{(1-\mu)}{\beta^2}\frac{\partial^2 w}{\partial Q^2}+\frac{6(1-2\mu)a^2}{t^2}.\left(1+\frac{1}{c}\right)=0 \quad (41)$$

This gives:

$$\frac{\partial^2 w}{\partial R^2}(1-\mu)+\frac{(1-\mu)}{\beta^2}\frac{\partial^2 w}{\partial Q^2}+\frac{6(1-2\mu)a^2}{t^2}.\left(1+\frac{1}{c}\right)=0 \quad (42)$$

Adding Equations 39 and 42 gives:

$$(1-\mu)\frac{\partial^2 w}{\partial R^2}+\frac{1}{\beta^2}.\frac{\partial^2 w}{\partial Q^2}(1-\mu)+\frac{6(1-2\mu)a^2}{t^2}.\left(1+\frac{1}{c}\right)+\frac{\partial^2 w}{\partial R^2}(1-\mu)+\frac{(1-\mu)}{\beta^2}\frac{\partial^2 w}{\partial Q^2}+\frac{6(1-2\mu)a^2}{t^2}.\left(1+\frac{1}{c}\right)=0 \quad (43)$$

This gives:

$$2(1-\mu)\frac{\partial^2 w}{\partial R^2}+\frac{2(1-\mu)}{\beta^2}\frac{\partial^2 w}{\partial Q^2}+\frac{12(1-2\mu)a^2}{t^2}.\left(1+\frac{1}{c}\right)=0 \quad (44)$$

This gives:

$$(1-\mu)\frac{\partial^2 w}{\partial R^2}+\frac{(1-\mu)}{\beta^2}\frac{\partial^2 w}{\partial Q^2}+\frac{6(1-2\mu)(1+c)a^2}{t^2}.\frac{1}{c}=0 \quad (45)$$

Rearranging Equation 45 gives:

$$\frac{6(1-2\mu)(1+c)}{t^2}=-\frac{c(1-\mu)}{a^2}\left(\frac{\partial^2 w}{\partial R^2}+\frac{1}{\beta^2}\frac{\partial^2 w}{\partial Q^2}\right) \quad (46)$$

2.7. Governing Equation

The minimization of the total potential energy functional with respect to deflection (w) gives the equilibrium equation (Governing Equation) along the z-axis as presented in Equation 47. That is:

$$\frac{\partial \Pi}{\partial w}=\frac{D^*}{2a^2}\int_0^1\int_0^1\left[\frac{12(1-2\mu)}{t^2}\left(\frac{\partial^2 w}{\partial R^2}+\frac{1}{\beta^2}.\frac{\partial^2 w}{\partial Q^2}+a.\frac{\partial \theta_x}{\partial R}+\frac{a}{\beta}\frac{\partial \theta_y}{\partial Q}\right)+2\frac{(1-\mu)a^2}{t^4}.\frac{\partial^2 w}{\partial S^2}-2\frac{N_x}{D^*}.\frac{\partial^2 w}{\partial R^2}\right]dR\,dQ=0 \quad (47)$$

Substituting Equations 29 and 30 into Equation 47 and simplifying the outcome gives:

$$\frac{D^*}{2a^2}\int_0^1\int_0^1\left[\frac{6(1-2\mu)(1+c)}{t^2}\left(\frac{\partial^2 w}{\partial R^2}+\frac{1}{\beta^2}.\frac{\partial^2 w}{\partial Q^2}\right)+\frac{(1-\mu)a^2}{t^4}\frac{\partial^2 w}{\partial S^2}-\frac{N_x}{D^*}.\frac{\partial^2 w}{\partial R^2}\right]dR\,dQ=0 \quad (48)$$

Substituting Equation 46 into Equation 48 and simplifying the outcome gives:

$$\frac{D^*}{2a^4}\int_0^1\int_0^1\left[\left(\frac{\partial^4 w}{\partial R^4}+\frac{2}{\beta^2}.\frac{\partial^4 w}{\partial R^2\partial Q^2}+\frac{1}{\beta^4}.\frac{\partial^4 w}{\partial Q^4}\right)+\frac{(1-\mu)a^4}{gt^4}.\frac{\partial^2 w}{\partial S^2}-\frac{N_x a^4}{gD^*}.\frac{\partial^2 w}{\partial R^2}\right]dR\,dQ=0 \quad (49)$$

Given that g is the shear deformation profile (shear deformation line), let;

$$g=g(z)=c(1-\mu) \quad (50)$$

Assuming the solution to be separable, it can be written that:

$$w(R,Q,S)=w_R(R).w_Q(Q).w_S(S) \quad (51)$$

More so, let the deflection be defined as:

$$w(x,y,z)=w_1(x,y).w_S(z) \quad (52)$$

Where:

$$w_1(x,y)=w_R(x).w_Q(y) \quad (53)$$

Substituting Equation 53 into Equation 49 gives:

$$\frac{D^*}{2a^4}\int_0^1\int_0^1\left[\left(\frac{\partial^4 w_1}{\partial R^4}+\frac{2}{\beta^2}.\frac{\partial^4 w_1}{\partial R^2\partial Q^2}+\frac{1}{\beta^4}.\frac{\partial^4 w_1}{\partial Q^4}\right)w_S+w_1\frac{(1-\mu)a^4}{gt^4}.\frac{\partial^2 w_S}{\partial S^2}-w_S\frac{N_x a^4}{gD^*}.\frac{\partial^2 w_1}{\partial R^2}\right]dR\,dQ=0 \quad (54)$$

Rearranging Equation 54 gives:

$$\frac{D^*}{2a^4}\int_0^1\int_0^1\left[\left(\frac{\partial^4 w_1}{\partial R^4}+\frac{2}{\beta^2}.\frac{\partial^4 w_1}{\partial R^2\partial Q^2}+\frac{1}{\beta^4}.\frac{\partial^4 w_1}{\partial Q^4}-\frac{N_{x1}a^4}{gD^*}.\frac{\partial^2 w_1}{\partial R^2}\right)w_S+\frac{w_1}{g}\left(\frac{(1-\mu)a^4}{t^4}.\frac{\partial^2 w_S}{\partial S^2}\right)\right]dR\,dQ=0 \quad (55)$$

For Equation 55 to be true, its integrand can be zero. That is:

$$\left(\frac{\partial^4 w_1}{\partial R^4}+\frac{2}{\beta^2}.\frac{\partial^4 w_1}{\partial R^2\partial Q^2}+\frac{1}{\beta^4}.\frac{\partial^4 w_1}{\partial Q^4}-\frac{N_{x1}a^4}{gD^*}.\frac{\partial^2 w_1}{\partial R^2}\right)w_S+\frac{w_1}{g}\left(\frac{(1-\mu)a^4}{t^4}.\frac{\partial^2 w_S}{\partial S^2}\right)=0 \quad (56)$$

One of the possibilities of Equation 56 to be true is for the terms in each of the two brackets sum to zero. That is:

$$\frac{\partial^4 w_1}{\partial R^4} + \frac{2}{\beta^2}.\frac{\partial^4 w_1}{\partial R^2 \partial Q^2} + \frac{1}{\beta^4}.\frac{\partial^4 w_1}{\partial Q^4} - \frac{N_{x1} a^4}{gD^*}.\frac{\partial^2 w_1}{\partial R^2} = 0 \quad (57)$$

$$\frac{(1-\mu)a^4}{t^4}.\frac{\partial^2 w_S}{\partial S^2} = 0 \quad (58)$$

Equations 57 and 58 are the two governing equations of a 3-dimensional rectangular plate subject to pure buckling.

2.8. Solution to Governing Equation

The numerical solution to the governing equation is obtained by solving Equation 57. This was done by integrating Equation 57 with respect to R and Q to yield Equation in Equation 57 and 58. This Equation 57 and 58, when solved gives an exact solution to the differential equation for deflection and buckling load (67a, b) and 90 or 91 respectively. This Equation (67a, b) becomes the general characteristic equation which is an expression that when subjected to a particular boundary condition will yield a particular solution for the deflection in Equation (92a, b). The exact solution to the differential equation of 57 in trigonometric form is:

$$w_1 = [1 \quad R \quad Cos\,(c_1 R) \quad Sin\,(c_1 R)] \begin{bmatrix} a_0 \\ a_1 \\ a_2 \\ a_3 \end{bmatrix} . [1 \quad Q \quad Cos\,(c_1 Q) \quad Sin\,(c_1 Q)] \begin{bmatrix} b_0 \\ b_1 \\ b_2 \\ b_3 \end{bmatrix} \quad (59a)$$

The approximate solution to the differential equation of Equation 57 in polynomial form as:

$$w_1 = (1 \quad R \quad R^2 R^3 R^4) \begin{bmatrix} a_0 \\ a_1 \\ a_2 \\ a_3 \\ a_4 \end{bmatrix} . (1 \quad Q \quad Q^2 Q^3 Q^4) \begin{bmatrix} b_0 \\ b_1 \\ b_2 \\ b_3 \\ b_4 \end{bmatrix} \quad (59b)$$

In a more symbolized form, Equation 59(a, b) becomes:

$$w_1 = \mathrm{h_R A_R}.\mathrm{h_Q A_Q} \quad (60)$$

Rearranging Equation 60 by bringing all the constants in one place and variable in another place gives:

$$w = (A_R.A_Q).(h_R h_Q) \quad (61)$$

The governing equations as obtained in Equation 58 will be solved to get the value of the constant (Δ_0). The non-trivial possibilities of Equation 58 to be true is for:

$$\frac{\partial^2 w_S}{\partial S^2} = 0 \quad (62)$$

Integrating Equation 62 once with respect to S gives:

$$\frac{\partial w_S}{\partial S} = \Delta_1 \quad (63)$$

Integrating Equation 63 gives:

$$w_S = \Delta_0 + \Delta_1 S \quad (64)$$

Where: Δ_0 and Δ_1 are constants of integration. At the extreme fibers (where S = ±0.5) the straining of the plate along z axis is allowed. However, the middle fiber (where S = 0) of the plate, straining of the plate along z axis is zero. Thus, at the middle fiber, Equation 73 is zero. Equation 73 is the strain along z-axis. That is: at middle fiber;

$$\Delta_1 = 0 \quad (65)$$

Substituting Equation 74 into Equation 73 gives:

$$w_S = \Delta_0 \quad (66)$$

Equation 66 implies that z-strip deflection of the middle surface of the plate is actually a constant and not a

variable (or a function). Thus, it could be concluded that the theory reduces to Mindlin's plate theory with the bending stiffness D* in place of D (see Equations (23a, b)).

Substituting Equations 59a and 66 into Equation 52 gives:

$$w = \Delta_0[1 \quad R \quad Cos\,(c_1R) \;\; Sin\,(c_1R)]\begin{bmatrix}a_0\\a_1\\a_2\\a_3\end{bmatrix}.[1 \quad Q \quad Cos\,(c_1Q) \;\; Sin\,(c_1Q)]\begin{bmatrix}b_0\\b_1\\b_2\\b_3\end{bmatrix} \tag{67a}$$

Substituting Equations 59b and 66 into Equation 52 gives:

$$w = \Delta_0\,[1 \;\; R \;\; R^2R^3R^4]\begin{bmatrix}a_0\\a_1\\a_2\\a_3\\a_4\end{bmatrix}.[1 \;\; Q \;\; Q^2Q^3Q^4]\begin{bmatrix}b_0\\b_1\\b_2\\b_3\\b_4\end{bmatrix} \tag{67b}$$

Substituting Equation 67a into Equations 29 and simplifying the outcome gives:

$$\theta_x = \frac{c}{a}.\Delta_0.[1 \quad c_1Sin\,(c_1R) \;\; c_1Cos\,(c_1R)]\begin{bmatrix}a_1\\a_2\\a_3\end{bmatrix}.[1 \quad Q \quad Cos\,(c_1Q) \;\; Sin\,(c_1Q)]\begin{bmatrix}b_0\\b_1\\b_2\\b_3\end{bmatrix} \tag{68a}$$

Substituting Equation 67b into Equations 29 and simplifying the outcome gives:

$$\theta_x = \frac{c}{a}.\Delta_0.[1 \;\; 2R \;\; 3R^2 \;\; 4R^3]\begin{bmatrix}a_1\\a_2\\a_3\\a_4\end{bmatrix}.[1 \;\; Q \;\; Q^2Q^3Q^4]\begin{bmatrix}b_0\\b_1\\b_2\\b_3\\b_4\end{bmatrix} \tag{68b}$$

Substituting Equation 67a into Equations 30 and simplifying the outcome gives:

$$\theta_y = \frac{c}{a\beta}.\Delta_0.[1 \quad R \quad Cos\,(c_1R) \;\; Sin\,(c_1R)]\begin{bmatrix}a_0\\a_1\\a_2\\a_3\end{bmatrix}.[1 \quad c_1Sin\,(c_1Q) \;\; c_1Cos\,(c_1Q)]\begin{bmatrix}b_1\\b_2\\b_3\end{bmatrix} \tag{69a}$$

Substituting Equation 67b into Equations 30 and simplifying the outcome gives:

$$\theta_y = \frac{c}{a\beta}.\Delta_0.[1 \;\; R \;\; R^2R^3R^4]\begin{bmatrix}a_0\\a_1\\a_2\\a_3\\a_4\end{bmatrix}.[1 \;\; 2Q \;\; 3Q^2 \;\; 4Q^3]\begin{bmatrix}b_1\\b_2\\b_3\\b_4\end{bmatrix} \tag{69b}$$

In symbolic forms, Equations ($68a$ *and* $68b$) are:

$$\theta_x = \frac{A_{2R}}{a}.\frac{\partial h}{\partial R} \tag{70}$$

In symbolic forms, Equations 69 (a and b) are:

$$\theta_y = \frac{A_{2Q}}{a\beta}.\frac{\partial h}{\partial Q} \tag{71}$$

Where:

$$A_{2R} = c.\Delta_0.\frac{\partial h}{\partial R}.A_Q \tag{72}$$

$$A_{2Q} = c.\Delta_0\frac{\partial h}{\partial Q}.A_R \tag{73}$$

The constants c, Δ_0, A_R and A_Q whose values are unknown, will aid the solution of direct governing equation. Therefore, substituting Equations 52, 61, 70 and 71 into Equation 26, simplifying and factorizing the outcome gives:

$$\begin{aligned}\prod = \frac{D^*ab}{2a^4}\int_0^1\int_0^1\Big[&(1-\mu){A_{2R}}^2\left(\frac{\partial^2 h}{\partial R^2}\right)^2 + \frac{1}{\beta^2}\Big[A_{2R}.A_{2Q} + \frac{(1-2\mu){A_{2R}}^2}{2} + \frac{(1-2\mu){A_{2Q}}^2}{2}\Big]\left(\frac{\partial^2 h}{\partial R\,\partial Q}\right)^2 + \frac{(1-\mu){A_{2Q}}^2}{\beta^4}\left(\frac{\partial^2 h}{\partial Q^2}\right)^2 + \\ &6(1-2\mu)\left(\frac{a}{t}\right)^2\left(\Big[{A_{2R}}^2 + {A_1}^2 + 2A_1A_{2R}\Big].\left(\frac{\partial h}{\partial R}\right)^2 + \frac{1}{\beta^2}.\Big[{A_{2Q}}^2 + {A_1}^2 + 2A_1A_{2Q}\Big].\left(\frac{\partial h}{\partial Q}\right)^2\right) - \frac{N_x a^2 {A_1}^2}{D^*}.\left(\frac{\partial h}{\partial R}\right)^2\Big]\,dR\,dQ\end{aligned} \tag{74}$$

Writing Equation 74 in more symbolized form gives:

$$\prod = \frac{D^* ab}{2a^4}\left[(1-\mu){A_{2R}}^2 k_{RR} + \frac{1}{\beta^2}\left[A_{2R}.A_{2Q} + \frac{(1-2\mu){A_{2R}}^2}{2} + \frac{(1-2\mu){A_{2Q}}^2}{2}\right]k_{RQ} + \frac{(1-\mu){A_{2Q}}^2}{\beta^4}k_{QQ} + 6(1-2\mu)\left(\frac{a}{t}\right)^2\left(\left[{A_{2R}}^2 + {A_1}^2 + 2A_1A_{2R}\right].k_R + \frac{1}{\beta^2}.\left[{A_{2Q}}^2 + {A_1}^2 + 2A_1A_{2Q}\right].k_Q\right) - \frac{N_x a^2 {A_1}^2}{D^*}.k_R\right] \quad (75)$$

Where:

$$k_{RR} = \int_0^1\int_0^1\left(\frac{\partial^2 h}{\partial R^2}\right)^2 dRdQ;\ k_{RQ} = \int_0^1\int_0^1\left(\frac{\partial^2 h}{\partial R\partial Q}\right)^2 dRdQ;\ k_{QQ} = \int_0^1\int_0^1\left(\frac{\partial^2 h}{\partial Q^2}\right)^2 dRdQ;$$

$$k_R = \int_0^1\int_0^1\left(\frac{\partial h}{\partial R}\right)^2 dRdQ;\ k_Q = \int_0^1\int_0^1\left(\frac{\partial h}{\partial Q}\right)^2 dRdQ$$

Minimizing Equation 75 with respect to A_{2R} gives:

$$(1-\mu)A_{2R}k_{RR} + \frac{1}{2\beta^2}\left[A_{2Q} + A_{2R}(1-2\mu)\right]k_{RQ} + 6(1-2\mu)\left(\frac{a}{t}\right)^2[A_{2R} + A_1].k_R = 0 \quad (76)$$

Minimizing Equation 75 with respect to A_{2Q} gives:

$$\frac{(1-\mu)A_{2Q}}{\beta^4}k_{QQ} + \frac{1}{2\beta^2}\left[A_{2R} + A_{2Q}(1-2\mu)\right]k_{RQ} + \frac{6}{\beta^2}(1-2\mu)\left(\frac{a}{t}\right)^2\left([A_{2Q} + A_1].k_Q\right) = 0 \quad (77)$$

Rewriting Equations 76 and 77 gives:

$$\left[(1-\mu)k_{RR} + \frac{1}{2\beta^2}(1-2\mu)k_{RQ} + 6(1-2\mu)\left(\frac{a}{t}\right)^2 k_R\right]A_{2R} + \left[\frac{1}{2\beta^2}k_{RQ}\right]A_{2Q} = \left[-6(1-2\mu)\left(\frac{a}{t}\right)^2 k_R\right]A_1 \quad (78)$$

$$\left[\frac{1}{2\beta^2}k_{RQ}\right]A_{2R} + \left[\frac{(1-\mu)}{\beta^4}k_{QQ} + \frac{1}{2\beta^2}(1-2\mu)k_{RQ} + \frac{6}{\beta^2}(1-2\mu)\left(\frac{a}{t}\right)^2 k_Q\right]A_{2Q} = \left[-\frac{6}{\beta^2}(1-2\mu)\left(\frac{a}{t}\right)^2 k_Q\right]A_1 \quad (79)$$

Solving Equations 78 and 79 simultaneously gives:

$$A_{2R} = G_2A_1 \quad (80)$$

$$A_{2Q} = G_3A_1 \quad \text{Let:} \quad (81)$$

$$G_2 = \frac{(c_{12}c_{23} - c_{13}c_{22})}{(c_{12}c_{12} - c_{11}c_{22})} \quad (82)$$

$$G_3 = \frac{(c_{12}c_{13} - c_{11}c_{23})}{(c_{12}c_{12} - c_{11}c_{22})} \quad (83)$$

$$c_{11} = (1-\mu)k_{RR} + \frac{1}{2\beta^2}(1-2\mu)k_{RQ} + 6(1-2\mu)\left(\frac{a}{t}\right)^2 k_R \quad (84)$$

$$c_{22} = \frac{(1-\mu)}{\beta^4}k_{QQ} + \frac{1}{2\beta^2}(1-2\mu)k_{RQ} + \frac{6}{\beta^2}(1-2\mu)\left(\frac{a}{t}\right)^2 k_Q \quad (85)$$

$$c_{12} = c_{21} = \frac{1}{2\beta^2}k_{RQ};\ c_{13} = -6(1-2\mu)\left(\frac{a}{t}\right)^2 k_R;\ c_{23} = c_{32} = -\frac{6}{\beta^2}(1-2\mu)\left(\frac{a}{t}\right)^2 k_Q \quad (86)$$

Minimizing Equation 75 with respect to A_1 gives:

$$\frac{\partial \Pi}{\partial A_1} = \frac{D^* ab}{2a^4}\left[6(1-2\mu)\left(\frac{a}{t}\right)^2\left([2A_1 + 2A_{2R}].k_R + \frac{1}{\beta^2}.[2A_1 + 2A_{2Q}].k_Q\right) - 2\frac{N_x a^2 A_1}{D^*}.k_R\right] = 0 \quad (87)$$

This gives:

$$6(1-2\mu)\left(\frac{a}{t}\right)^2\left([A_1 + G_2A_1].k_R + \frac{1}{\beta^2}.[A_1 + G_3A_1].k_Q\right) - \frac{N_x a^2 A_1}{D^*}.k_R = 0 \quad (88)$$

Dividing Equation 88 through A_1 gives:

$$6(1-2\mu)\left(\frac{a}{t}\right)^2\left([1+G_2].k_R+\frac{1}{\beta^2}.[1+G_3].k_Q\right)-\frac{N_x a^2}{D^*}.k_R=0 \quad (89)$$

Rearranging Equation 89 and divided by π^2 gives:

$$\frac{N_x a^2}{\pi^2 D^*}=6(1-2\mu)\left(\frac{a}{t}\right)^2\left([1+G_2]+\frac{1}{\beta^2}.[1+G_3].\frac{k_Q}{k_R}\right) \quad (90)$$

Rearranging Equation 89 and using Equation 23, yields:

$$\frac{N_x a^2}{Et^3}=\frac{(1+\mu)}{2}\left(\frac{a}{t}\right)^2\left([1+G_2]+\frac{1}{\beta^2}.[1+G_3].\frac{k_Q}{k_R}\right) \quad (91)$$

2.9. Numerical Problem

Determine the critical buckling Load of the rectangular ssss plate shown on Figure 3 for various aspect ratios and span-depth ratio. The Poisson's ratio of the plate is 0.25.

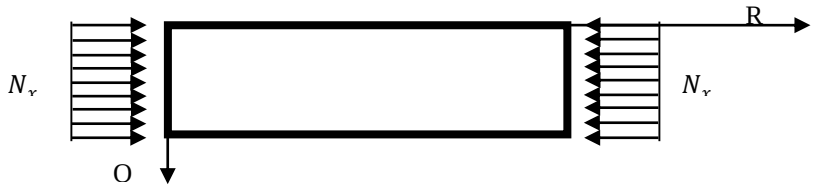

Figure 3. SSSS rectangular thick plate

The deflection functions in Equation (67a, b) after satisfying the boundary conditions in trigonometric and polynomial forms are presented in Equation (92a) and (92b) respectively as:

$$w=ASin\,(\pi*R)Sin\,(\pi*Q) \quad (92a)$$

$$w=A(R-2R^3+R^4)(Q-2Q^3+Q^4) \quad (92b)$$

The stiffness coefficients for the trigonometric and polynomial deflection functions are presented on Table 1.

Table 1. Stiffness coefficients of SSSS plate for trigonometric and polynomial forms of deflection function

Deflection form	k_{RR}	k_{RQ}	k_{QQ}	k_R	k_Q
Trigonometry	$\frac{\pi^4}{4}$	$\frac{\pi^4}{4}$	$\frac{\pi^4}{4}$	$\frac{\pi^2}{4}$	$\frac{\pi^2}{4}$
Polynomial	0.23619	0.235919	0.23619	0.0239	0.0239

3. Results and Discussions

As an indication of the error involved in using the classical plate theory, FSDT and HSDT for thick plate analysis, consider the problem of all edges simply supported square plate subjected to a uniformly distributed uniaxial compressive load presented in the Figure 3. A numerical result of the analysis is presented using the established equation from the previous section. Equation 90 and 91 were used to obtain the numerical value of the critical buckling load of the 3-D thick rectangular plate at varying stiffness, span to thickness ratio (a/t) and aspect ratio ($\beta = b/a$) of the plate.

For the non-dimensional values obtained in Tables 2 (considering Equation 90), it reveals that the values of critical buckling load increase as the span- thickness ratio increases. At the span to thickness ratio of 5 (Considering Equation 90), the present theory predicts the buckling load of 3.7582 using trigonometric (Trig.) displacement function and predicts 3.7604 using the polynomial (poly.) functions in the analysis. Similarly, at the span to thickness ratio of 10, the present theory predicts the buckling load of 4.2884 using trigonometric (Trig.) displacement function and predicts 4.2913 using the polynomial (poly.) functions in the analysis. The result of trigonometric function being lower is quite expected because they predict more exact solution and are economical in use compared to the polynomial whose exact function tends to infinity. This shows that as the thickness of the plate decreases, the critical buckling load increases. It can be deduced that, thinner the plate more failure tendency results.

Table 2. Non-dimensional critical buckling loads of square plate from various thick plate theories

a/t	Theories	Scholars	$\frac{N_x a^2}{\pi^2 D}$	%Diff (Trig)	%Diff (Poly)
5	Present 3-D plate theory (Trig.)	Present	3.7582		
	Present 3-D plate theory (Poly.)	Present	3.7604		
	Alternative II thick plate	Ibearugbulem et al. (2020) [23]	3.3682	10.38	10.43
	ESDT thick plate	Sayyad and Y. M. Ghugal (2014) [17]	3.2653	13.12	13.17
	FSDT thick plate	Shufrin, and M. Eisenberger (2005) [14]	3.2637	13.16	13.21
	HSDT thick plate	Reddy and N. D. Phan (1985) [19]	3.2653	13.12	13.17
10	Present 3-D plate theory (Trig.)	Present	4.2884		
	Present 3-D plate theory (Poly.)	Present	4.2913		
	Alternative II thick plate	Ibearugbulem et al. (2020) [23]	3.8220	10.88	10.94
	HPSDT thick plate	Sayyad and Y. M. Ghugal (2014) [17]	3.7866	11.70	11.76
	FSDT thick plate	Shufrin, and M. Eisenberger (2005) [14]	3.7866	11.70	11.76
	HSDT thick plate	Reddy and N. D. Phan (1985) [19]	3.7865	11.70	11.76
	CPT plate	Ibearugbulem (2016) [16]	4.0020	6.68	6.74

Comparing the result of the present study with those of CPT, FSDT and HSDT as presented in Table 2, it was discovered that as the span-thickness ratio increases, the results of the present study become closer to those obtained using the CPT [16], FSDT [14] and closest to those using other refined plate theory [19, 17, 21, 22, 24]. Then, it can be said that the values obtained are in agreement with those obtained in the literature. It is noticed that the present theory converges faster with RPT than the CPT and FSDT. This proved the reliability of the present model for thick plate analysis. Hence, confirming the accuracy and reliability of the derived relationships.

The credibility of the relationship is given in the percentage difference calculation presented in the Table 2. The average percentage difference between the present study ($at\ \mathrm{a/t} = 5$) using trigonometric function and those of [14, 19, 17, 23] is about 12.4% while the average percentage difference between the present study using the polynomial function and those of [14, 19, 17, 23] is 12.5%. This means that at the 87% confidence level, the values from the present study are the same with those from of previous studies. Similarly, the average percentage difference between the present study ($at\ \mathrm{a/t} = 10$) using trigonometric function and those of [14, 19, 17, 23] is about 11.5% while the average percentage difference between the present study using the polynomial function and those of [14, 19, 17, 23] is 11.6%. This means that at the 88 % confidence level, the values from the present study are the same with those from of previous studies.

Table 3. Comparison of the critical buckling load factor $\left(\frac{N_x a^2}{Et^3}\right)$ of a rectangular plate with various span to thickness ratio (a/t) and aspect ratio(β) under uniaxial load from different thick plate theories

a/t	Theories	β = b/a			
		1	1.5	2	2.5
5	Present study (Trig) [T]	3.2970	1.8023	1.3728	1.1916
	Present study (Poly) (P)	3.2990	1.8036	1.3739	1.1927
	Moslemi et al. (2016) [30]	3.1530	-	-	-
	Ezeh et al. (2018) [24]	2.9556	1.6255	1.2408	1.0783
	Gunjal et al. (2015) [22]	2.9490	1.6620	1.2380	1.0760
	Sayyad and Y. M. Ghugal [21]	3.0260	1.6540	1.2590	1.0930
	%Diff between T and P	0.06	0.07	0.08	0.09
	%Diff between T and [30]	4.37	-	-	-
	%Diff between T and [24]	10.35	9.81	9.62	9.51
	%Diff between T and [22]	10.56	7.78	9.82	9.70
	%Diff between T and [21]	8.22	8.23	8.29	8.27
10	Present study (Trig) [T]	3.7622	1.9883	1.496	1.2911
	Present study (Poly) (P)	3.7648	1.9899	1.4973	1.2924
	Moslemi et al. (2016) [30]	3.7412	-	-	-
	Ezeh et al. (2018) [24]	3.4249	1.8155	1.3668	1.1790

	Gunjal et al. (2015) [22]	3.4220	1.8120	1.3640	1.1780
	Sayyad and Y. M. Ghugal [21]	3.4540	1.8250	1.3730	1.1850
	%Diff between T and P	0.07	0.08	0.09	0.10
	%Diff between T and [30]	0.56	-	-	-
	%Diff between T and [24]	8.97	8.69	8.64	8.68
	%Diff between T and [22]	9.04	8.87	8.82	8.76
	%Diff between T and [21]	8.19	8.21	8.22	8.22
20	Present study (Trig) [T]	3.8997	2.041	1.5303	1.3186
	Present study (Poly) (P)	3.9025	2.0427	1.5317	1.3200
	Moslemi et al. (2016) [30]	3.9310	-	-	-
	Ezeh et al. (2018) [24]	3.5691	1.8704	1.4034	1.2088
	Gunjal et al. (2015) [22]	3.5650	1.8670	1.4000	1.2060
	Sayyad and Y. M. Ghugal [21]	3.5820	1.8740	1.4050	1.2110
	%Diff between T and P	0.07	0.08	0.09	0.11
	%Diff between T and [30]	0.80	-	-	-
	%Diff between T and [24]	8.48	8.36	8.29	8.33
	%Diff between T and [22]	8.58	8.53	8.51	8.54
	%Diff between T and [21]	8.15	8.18	8.19	8.16
100	Present study (Trig) [T]	3.9459	2.0585	1.5417	1.3277
	Present study (Poly) (P)	3.9488	2.0601	1.5431	1.3290
	Moslemi et al. (2016) [30]	3.9970	-	-	-
	Ezeh et al. (2018) [24]	3.6172	1.8887	1.4148	1.2179
	Gunjal et al. (2015) [22]	3.6130	1.8850	1.4120	1.2160
	Sayyad and Y. M. Ghugal [21]	3.6250	1.8910	1.4160	1.2190
	%Diff between T and P	0.07	0.08	0.09	0.08
	%Diff between T and [30]	1.30	-	-	-
	%Diff between T and [24]	8.33	8.25	8.23	8.27
	%Diff between T and [22]	8.44	8.43	8.41	8.41
	%Diff between T and [21]	8.13	8.14	8.15	8.19

Table 4. Comparison of the critical buckling load factor $\left(\frac{N_x a^2}{Et^3}\right)$ of a rectangular plate with various span to thickness ratio (a/t) and aspect ratio(β) under uniaxial load from different thick plate theories.

a/t	Theories	β = b/a			
		1	1.5	2	2.5
5	Present study (Poly) (P)	3.2990	1.8036	1.3739	1.1927
	Present study (Trig) [T]	3.2970	1.8023	1.3728	1.1916
	Moslemi et al. (2016) [30]	3.1530	-	-	-
	Ezeh et al. (2018) [24]	2.9556	1.6255	1.2408	1.0783
	Gunjal et al. (2015) [22]	2.9490	1.6620	1.2380	1.0760
	Sayyad and Y. M. Ghugal [21]	3.0260	1.6540	1.2590	1.0930
	%Diff between P and T	0.06	0.07	0.08	0.09
	%Diff between P and [30]	4.43	-	-	-
	%Diff between P and [24]	10.41	9.87	9.69	9.59
	%Diff between P and [22]	10.61	7.85	9.89	9.78
	%Diff between P and [21]	8.28	8.29	8.36	8.36
10	Present study (Poly) (P)	3.7648	1.9899	1.4973	1.2924
	Present study (Trig) [T]	3.7622	1.9883	1.496	1.2911
	Moslemi et al. (2016) [30]	3.7412	-	-	-
	Ezeh et al. (2018) [24]	3.4249	1.8155	1.3668	1.1790
	Gunjal et al. (2015) [22]	3.4220	1.8120	1.3640	1.1780
	Sayyad and Y. M. Ghugal [21]	3.4540	1.8250	1.3730	1.1850

	%Diff between P and T	0.07	0.08	0.09	0.10
	%Diff between P and [30]	0.63	-	-	-
	%Diff between P and [24]	9.03	8.76	8.72	8.77
	%Diff between P and [22]	9.11	8.94	8.90	8.85
	%Diff between P and [21]	8.26	8.29	8.30	8.31
	Present study (Poly) (P)	3.9025	2.0427	1.5317	1.3200
	Present study (Trig) [T]	3.8997	2.041	1.5303	1.3186
	Moslemi et al. (2016) [30]	3.9310	-	-	-
	Ezeh et al. (2018) [24]	3.5691	1.8704	1.4034	1.2088
	Gunjal et al. (2015) [22]	3.565	1.8670	1.4000	1.2060
20	Sayyad and Y. M. Ghugal [21]	3.582	1.8740	1.4050	1.2110
	%Diff between P and T	0.07	0.08	0.09	0.11
	%Diff between P and [30]	0.73	-	-	-
	%Diff between P and [24]	8.54	8.43	8.38	8.42
	%Diff between P and [22]	8.65	8.60	8.60	8.64
	%Diff between P and [21]	8.21	8.26	8.27	8.26
	Present study (Poly) (P)	3.9488	2.0601	1.5431	1.3290
	Present study (Trig) [T]	3.9459	2.0585	1.5417	1.3277
	Moslemi et al. (2016) [30]	3.9970	-	-	-
	Ezeh et al. (2018) [24]	3.6172	1.8887	1.4148	1.2179
	Gunjal et al. (2015) [22]	3.6130	1.8850	1.4120	1.2160
100	Sayyad and Y. M. Ghugal [21]	3.6250	1.8910	1.4160	1.2190
	%Diff between P and T	0.07	0.08	0.09	0.08
	%Diff between P and [30]	1.22	-	-	-
	%Diff between P and [24]	8.40	8.32	8.31	8.36
	%Diff between P and [22]	8.50	8.50	8.50	8.50
	%Diff between P and [21]	8.20	8.21	8.24	8.28

For the non-dimensional numerical result of the critical buckling load of the plate obtained at different stiffness, span to thickness ratio) ($a/t = 5, 10, 20\ and\ 100$) and aspect ratio ($\beta = 1.0, 1.5 \text{ and } 2.0$) using the established model (Equation 90 and 91) in the present study is presented in Tables 3 and 4. The result shows that the values of critical buckling load increase as the span- thickness ratio increases. Looking closely at Tables 3 and 4, it is shown that the increase in the value of the length-breadth ratio ($\beta = 1.0, 1.5 \text{ and } 2.0$) decreases the value of the critical buckling load. In other words, the increase in the width of the plate increases the failure tendency of the plate structure.

In order to evaluate the validity of the of this work, the present study are compared to those of the past studies using CPT, RPT (incomplete 3D) and 3D elasticity theory as presented in Table 3 and 4, a summary of the percentage difference evaluation are presented in the Table 5 and Table 6 for trigonometric and polynomial functions respectively. From Table 3, it finds that the average total percentage difference between the values from the present study using the trigonometric displacement function and those of the 3D elasticity theory [30] is about 0.89%, while the average total percentage difference between the values from the present study using the trigonometric displacement function and those of the incomplete 3D theory [21, 22, 24] is about 8.79%. Similarly, from Table 4, it finds that the average total percentage difference between the values from the present study using the trigonometric displacement function and those of the 3D elasticity theory [30] is about 0.91%, while the average total percentage difference between the values from the present study using the trigonometric displacement function and those of the incomplete 3D theory [21, 22, 24] is about 8.85%. This shows the coarseness of the incomplete 3-D plate theory in the thick plate analysis. Hence, it is shown that, all the recorded average percentage differences between trigonometric and polynomial approaches used in this work and those of 3D elasticity theory [30] is lower than 1.0%. These differences are insignificant, confirmed that the present theory provides a good solution for the 3D stability analysis of all types of a rectangular plate. Meanwhile, the average percentage differences between the present work (trig. and poly.) and those of incomplete 3D theory [21, 22, 24] is higher than 7.70%%. These differences being far higher than 5% are quite unacceptable in statistics and cannot be overlooked. Thus, confirming that the incomplete 3-D refined plate theory is unreliable for the stability analysis of thick rectangular plate.

Table 5. Percentage difference between the values of the critical buckling load factor $\left(\frac{N_x a^2}{Et^3}\right)$ of a rectangular square plate with various span to thickness ratio (a/t) under uniaxial load from present (Trigonometric) and past studies.

$$\%Diff = \frac{Absolute\ difference\ betwee\ present\ and\ past\ value}{Past\ value}$$

Span-to depth ratio (a/t)	%Diff between T and P	%Diff between T and [30]	%Diff between T and [24]	%Diff between T and [22]	%Diff between T and [21]
5	0.06	4.37	10.35	10.56	8.22
10	0.07	0.56	8.97	9.04	8.19
20	0.07	0.70	8.48	8.58	8.15
100	0.07	1.20	8.33	8.44	8.13
Average % Difference	0.07	1.71	9.03	9.16	8.17
Total % Difference	0.89			8.79	
	5.63				

Table 6. Percentage difference between the values of the critical buckling load factor $\left(\frac{N_x a^2}{Et^3}\right)$ of a rectangular square plate with various span to thickness ratio (a/t) under uniaxial load from present (Polynomial) and past studies.

$$\%Diff = \frac{Absolute\ difference\ betwee\ present\ and\ pasr\ value}{Past\ value}$$

Span-to depth ratio (a/t)	%Diff between P and T	%Diff between P and [30]	%Diff between P and [24]	%Diff between P and [22]	%Diff between P and [21]
5	0.06	4.43	10.41	10.61	8.28
10	0.07	0.63	9.03	9.11	8.26
20	0.07	0.73	8.54	8.65	8.21
100	0.07	1.22	8.40	8.50	8.20
Average % Difference	0.07	1.75	9.10	9.22	8.24
Total % Difference	0.91			8.85	
	5.68				

From Figures 4 to 13, comparison made from the present study and those from past scholars (RPT and incomplete 3D analysis) proves that, the incomplete three-dimensional shear deformation theory is only an approximate relation for buckling analysis of thick plate and cannot guarantee safety in a typical thick plate analysis. Furthermore, the trigonometric displacement functions developed to give a close form solution, thereby considered more accurate and safer for complete exact three-dimensional stability analysis of plate than the polynomial displacement function. Its use in the analysis of thick plates will yield almost an exact result. On the other hand, the polynomial displacement function which predicts a slightly higher value of average percentage difference gives an approximate solution whose exact value is tends to infinity.

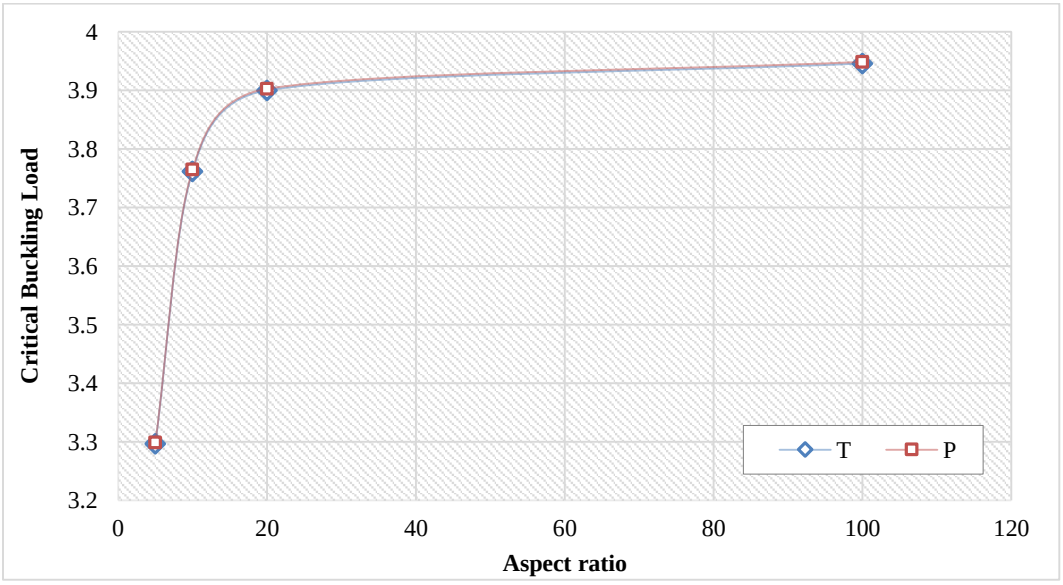

Figure 4. Graph of critical buckling load versus aspect ratio (a/t) for SSSS plate using trigonometric (T) and polynomial (P) of the present study

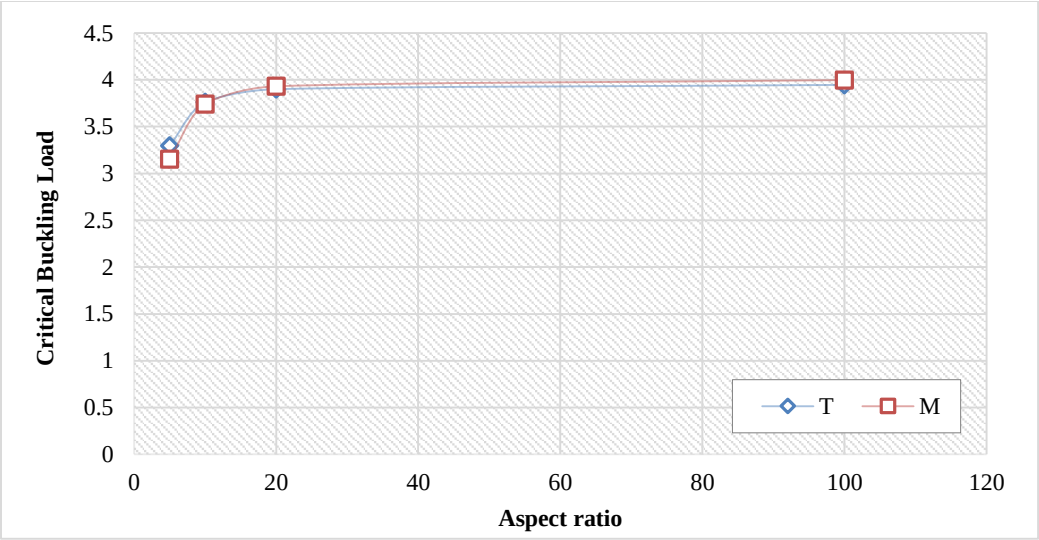

Figure 5. Graph of critical buckling load versus aspect ratio (a/t) for SSSS plate showing comparison between the present study (trigonometric) (T) and Moslemi et al. (2016) (M)

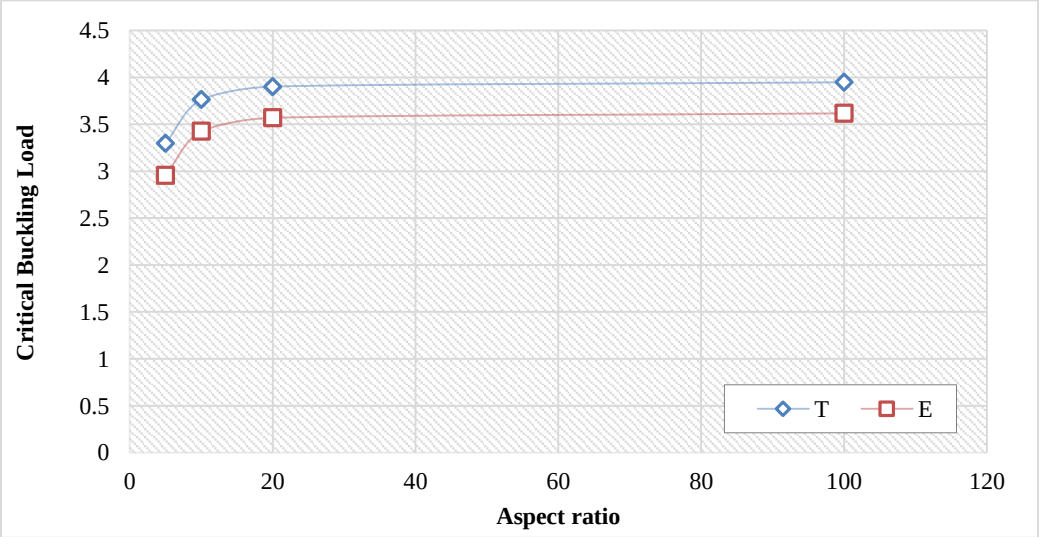

Figure 6. Graph of critical buckling load versus aspect ratio (a/t) for SSSS plate showing comparison between the present study (trigonometric) (T) and Ezeh et al. (2018) (E)

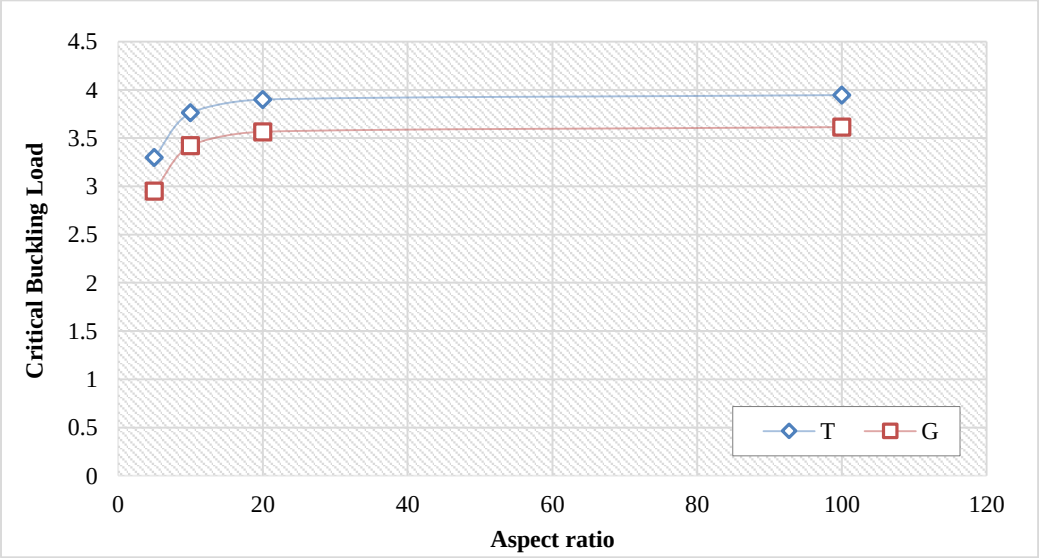

Figure 7. Graph of critical buckling load versus aspect ratio (a/t) for SSSS plate showing comparison between the present study (trigonometric) (T) and Gunjal et al. (2015) (G)

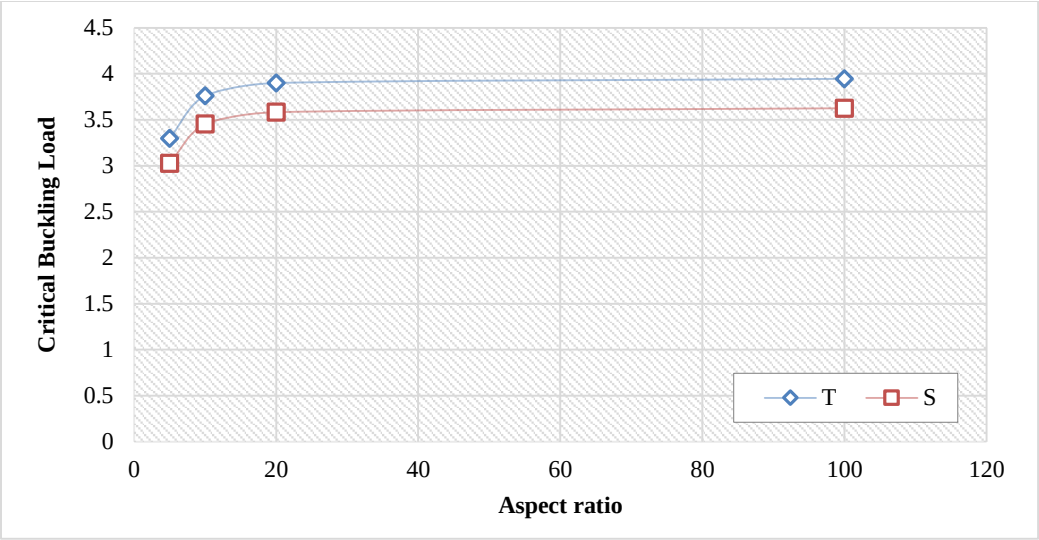

Figure 8. Graph of critical buckling load versus aspect ratio (a/t) for SSSS plate showing comparison between the present study (trigonometric) (T) and Sayaad and Ghugal (2012) (S)

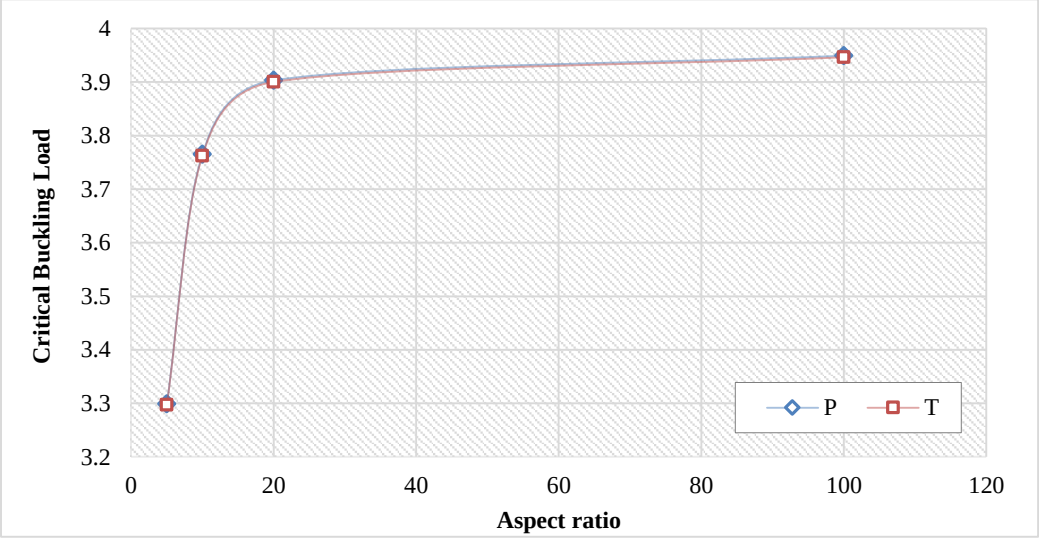

Figure 9. Graph of critical buckling load versus aspect ratio (a/t) for SSSS plate using polynomial (P) and trigonometric (T) of the present study

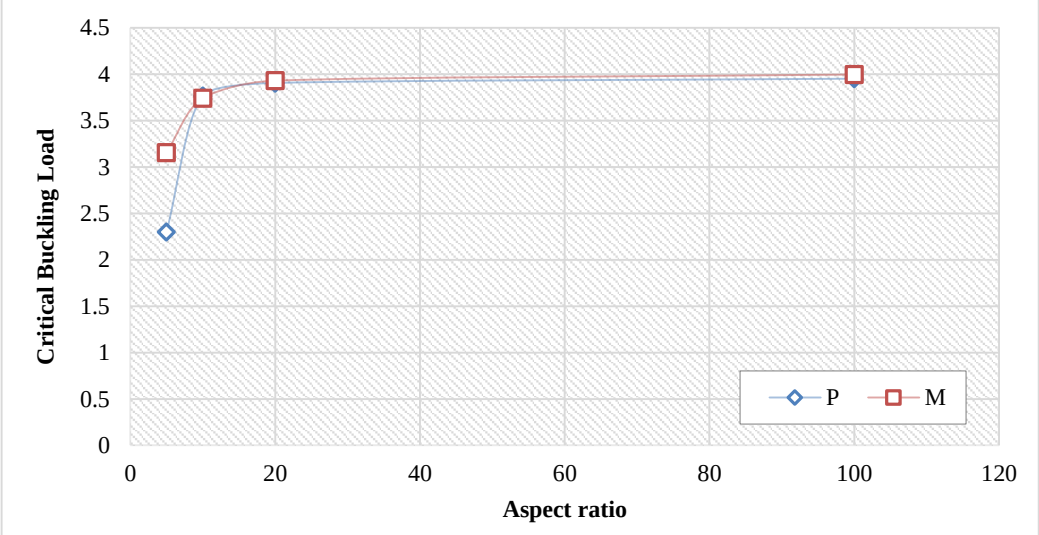

Figure 10. Graph of critical buckling load versus aspect ratio (a/t) for SSSS plate showing comparison between the present study polynomial (P) and Moslemi et al. (2016) (M)

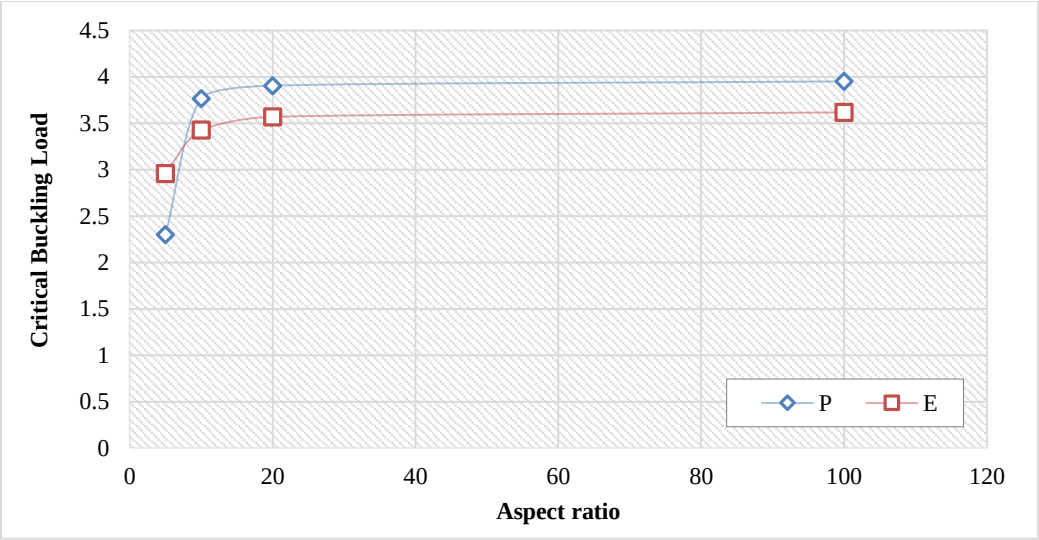

Figure 11. Graph of critical buckling load versus aspect ratio (a/t) for SSSS plate showing comparison between the present study polynomial (P) and Ezeh et al. (2018) (E)

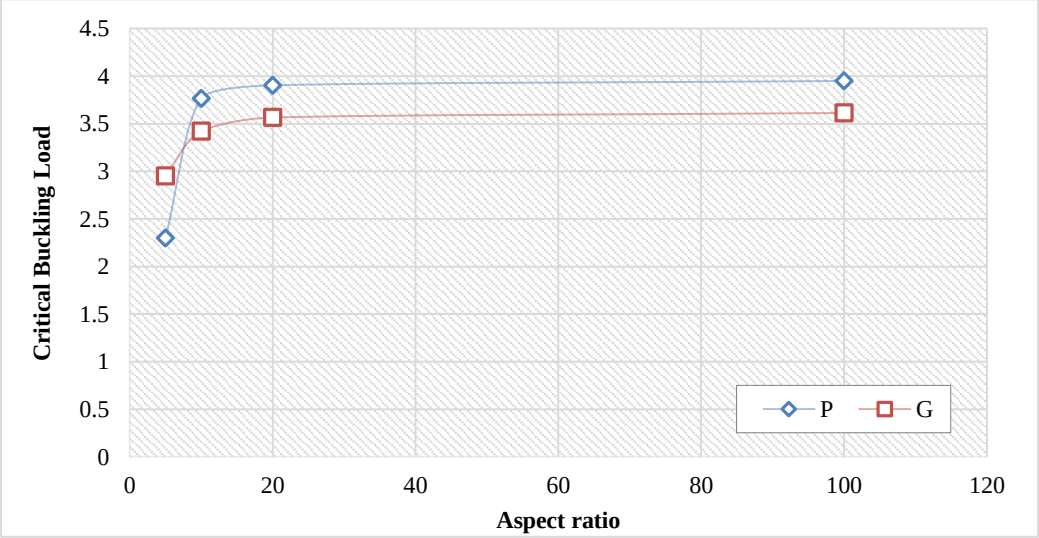

Figure 12. Graph of critical buckling load versus aspect ratio (a/t) for SSSS plate showing comparison between the present study polynomial (P) and Gunjal et al. (2015) (G)

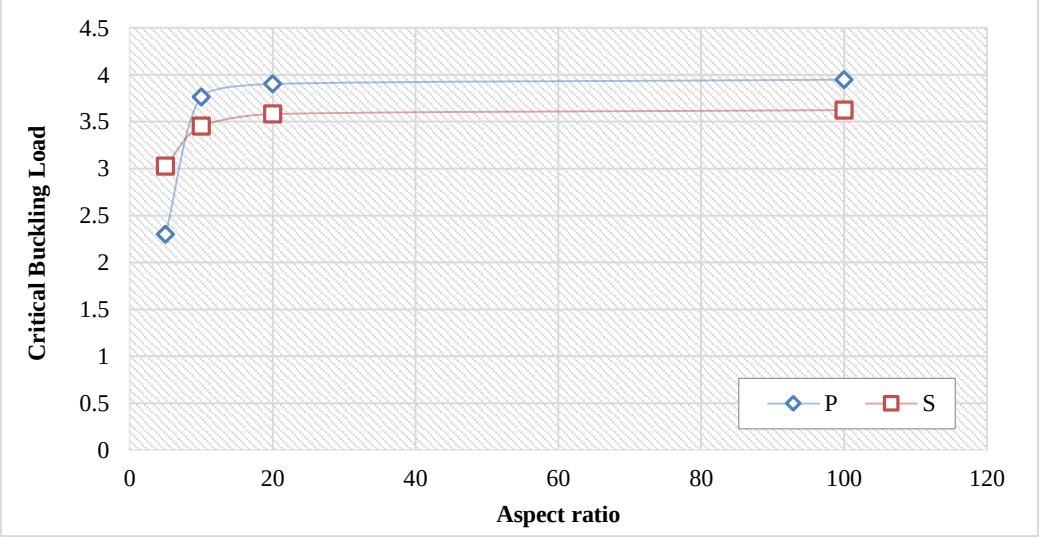

Figure 13. Graph of critical buckling load versus aspect ratio (a/t) for SSSS plate showing comparison between the present study polynomial (P) and Sayaad and Ghugal (2012) (S)

4. Conclusion

The 3-D exact theory is a plate theory that involves all the six strains $(\varepsilon_x, \varepsilon_v, \varepsilon_z, \gamma_{xv}, \gamma_{xz}\ and\ \gamma_{vz})$ and stress $(\sigma_x, \sigma_v, \sigma_z, \tau_{xv}, \tau_{xz}\ and\ \tau_{vz})$ components in the analysis. Hence, they include more modulus of elasticity (E) and other mechanical properties of the plate. As a consequence, the proposed 3-D approach always predicts buckling load greater than those predicted by CPT, FSDT and polynomial and non-polynomial higher-order plate theories because of these additional load (stresses), modulus of elasticity (E) and other mechanical properties of the plate. From the result of percentage difference recorded, it can be concluded that the classical theory is good for thin plates, but over-predicts buckling loads in relatively thick plates. Hence, the incomplete three-dimensional refined plate theory is only an approximate relation for buckling analysis of thick plate (although it turns out to be exact in the case of pure bending). Furthermore, the trigonometric displacement shear deformation theory developed to give a close form solution, thereby considered more accurate and safe for complete exact three-dimensional thick plate analysis than the polynomial. Its use in the analysis of thick plates will yield almost an exact result. On the other hand, the polynomial displacement function which predicts a slightly higher value of average percentage difference gives an approximate solution whose exact value is tends to infinity. Thus, confirming that the exact 3-D plate theory using polynomial and trigonometric displacement function provides a good solution for the stability analysis of plates and, can be recommended for analysis of any type of rectangular plate under the same loading and boundary condition.

5. Declarations

5.1. Author Contributions

Conceptualization, F.C.O., T.E.O. and B.O.M.; methodology, F.C.O., T.E.O. and B.O.M.; software, F.C.O., T.E.O. and B.O.M.; formal analysis, F.C.O., T.E.O. and B.O.M.; writing—original draft preparation, F.C.O., T.E.O. and B.O.M.; writing—review and editing, F.C.O., T.E.O. and B.O.M. All authors have read and agreed to the published version of the manuscript.

5.2. Data Availability Statement

The data presented in this study are available in article.

5.3. Funding

The authors received no financial support for the research, authorship, and/or publication of this article.

5.4. Acknowledgements

We would like to acknowledge Ibearugbulem, Owus Mathias of Federal University of Technology, Owerri, Nigeria for providing the technical assistance during this research.

5.5. Conflicts of Interest

The authors declare no conflict of interest.

6. References

[1] Reddy, J. N. (2006). Classical Theory of Plates. In Theory and Analysis of Elastic Plates and Shells, CRC Press. doi:10.1201/9780849384165-7.

[2] Onyeka, F. C., & Okeke, T. E. (2021). Analysis of critical imposed load of plate using variational calculus. Journal of Advances in Science and Engineering, 4(1), 13–23. doi:10.37121/jase.v4i1.125.

[3] Festus, O., Okeke, E. T., & John, W. (2020). Strain–Displacement expressions and their effect on the deflection and strength of plate. Advances in Science, Technology and Engineering Systems, 5(5), 401–413. doi:10.25046/AJ050551.

[4] Shufrin, I., & Eisenberger, M. (2005). Stability and vibration of shear deformable plates - First order and higher order analyses. International Journal of Solids and Structures, 42(3–4), 1225–1251. doi:10.1016/j.ijsolstr.2004.06.067.

[5] Timoshenko, S. P., Gere, J. M., & Prager, W. (1962). Theory of Elastic Stability, Second Edition. In Journal of Applied Mechanics (2nd ed., Vol. 29, Issue 1). McGraw-Hill Books Company. doi:10.1115/1.3636481.

[6] Onyeka, F. C. (2020). Critical Lateral Load Analysis of Rectangular Plate Considering Shear Deformation Effect. Global Journal of Civil Engineering, 1, 16–27. doi:10.37516/global.j.civ.eng.2020.0121.

[7] Kirchhoff, G. (1850). 4. Über das Gleichgewicht und die Bewegung einer elastischen Scheibe. Journal Fur Die Reine Und Angewandte Mathematik, 1850(40), 51–88. doi:10.1515/crll.1850.40.51.

[8] Zenkour, A. M. (2003). Exact mixed-classical solutions for the bending analysis of shear deformable rectangular plates. Applied Mathematical Modelling, 27(7), 515–534. doi:10.1016/S0307-904X(03)00046-5.

[9] Reissner, E. (1944). On the Theory of Bending of Elastic Plates. Journal of Mathematics and Physics, 23(1–4), 184–191. doi:10.1002/sapm1944231184.

[10] Reissner, E. (1945). The Effect of Transverse Shear Deformation on the Bending of Elastic Plates. Journal of Applied Mechanics, 12(2), A69–A77. doi:10.1115/1.4009435.

[11] Mindlin, R. D. (1951). Influence of Rotatory Inertia and Shear on Flexural Motions of Isotropic, Elastic Plates. Journal of Applied Mechanics, 18(1), 31–38. doi:10.1115/1.4010217.

[12] Sadrnejad, S. A., Daryan, A. S., & Ziaei, M. (2009). Vibration equations of thick rectangular plates using mindlin plate theory. Journal of Computer Science, 5(11), 838–842. doi:10.3844/jcssp.2009.838.842.

[13] Ghugal, Y. M., & Sayyad, A. S. (2011). Free vibration of thick orthotropic plates using trigonometric shear deformation theory. Latin American Journal of Solids and Structures, 8(3), 229–243. doi:10.1590/S1679-78252011000300002.

[14] Shufrin, I., & Eisenberger, M. (2005). Stability and vibration of shear deformable plates - First order and higher order analyses. International Journal of Solids and Structures, 42(3–4), 1225–1251. doi:10.1016/j.ijsolstr.2004.06.067.

[15] Reissner, E. (1979). Note on the effect of transverse shear deformation in laminated anisotropic plates. Computer Methods in Applied Mechanics and Engineering, 20(2), 203–209. doi:10.1016/0045-7825(79)90018-5.

[16] Owus M, I. (2016). Use of Polynomial Shape Function in Shear Deformation Theory for Thick Plate Analysis. IOSR Journal of Engineering, 06(06), 08–20. doi:10.9790/3021-066010820.

[17] Festus, O., & Okeke, E. T. (2021). Analytical Solution of Thick Rectangular Plate with Clamped and Free Support Boundary Condition using Polynomial Shear Deformation Theory. Advances in Science, Technology and Engineering Systems Journal, 6(1), 1427–1439. doi:10.25046/aj0601162.

[18] Senjanović, I., Tomić, M., Vladimir, N., & Cho, D. S. (2013). Analytical solution for free vibrations of a moderately thick rectangular plate. Mathematical Problems in Engineering, 2013(3), 1–13. doi:10.1155/2013/207460.

[19] Reddy, J. N., & Phan, N. D. (1985). Stability and vibration of isotropic, orthotropic and laminated plates according to a higher-order shear deformation theory. Journal of Sound and Vibration, 98(2), 157–170. doi:10.1016/0022-460X(85)90383-9.

[20] Sayyad, A. S., & Ghugal, Y. M. (2014). Buckling and free vibration analysis of orthotropic plates by using exponential shear deformation theory. Latin American Journal of Solids and Structures, 11(8), 1298–1314. doi:10.1590/S1679-78252014000800001.

[21] Sayyad, A. S., & Ghugal, Y. M. (2013). Buckling analysis of thick isotropic plates by using exponential shear deformation theory. Applied and Computational Mechanics, 6, 185–196.

[22] Gunjal, S. M., Hajare, R. B., Sayyad, A. S., & Ghodle, M. D. (2015). Buckling analysis of thick plates using refined trigonometric shear deformation theory. Journal of Materials and Engineering Structures, 2, 159–167.

[23] Ibearugbulem, O. M., Ebirim, S. I., Anya, U. C., & Ettu, L. O. (2020). Application of alternative II theory to vibration and stability analysis of thick rectangular plates (Isotropic and orthotropic). Nigerian Journal of Technology, 39(1), 52–62. doi:10.4314/njt.v39i1.6.

[24] Ezeh, J. C., Onyechere, I. C., Ibearugbulem, O. M., Anya, U. C., & Anyaogu, L. (2018). Buckling Analysis of Thick Rectangular Flat SSSS Plates using Polynomial Displacement Functions. International Journal of Scientific and Engineering Research, 9(9), 387–392.

[25] Higdon, R. A., & Holl, D. L. (1937). Stresses in moderately thick rectangular plates. In Duke Mathematical Journal (Vol. 3, Issue 1). Iowa State University. doi:10.1215/S0012-7094-37-00303-X.

[26] Pagano, N. J. (1970). Exact Solutions for Rectangular Bidirectional Composites and Sandwich Plates. Journal of Composite Materials, 4(1), 20–34. doi:10.1177/002199837000400102.

[27] Uymaz, B., & Aydogdu, M. (2013). Three dimensional shear buckling of FG plates with various boundary conditions. Composite Structures, 96, 670–682. doi:10.1016/j.compstruct.2012.08.031.

[28] Singh, D. B., & Singh, B. N. (2016). Buckling analysis of three dimensional braided composite plates under uniaxial loading using Inverse Hyperbolic Shear Deformation Theory. Composite Structures, 157, 360–365. doi:10.1016/j.compstruct.2016.08.029.

[29] Lee, C. W. (1967). A three-dimensional solution for simply supported thick rectangular plates. Nuclear Engineering and Design, 6(2), 155–162. doi:10.1016/0029-5493(67)90126-4.

[30] Moslemi, A., Navayi Neya, B., & Vaseghi Amiri, J. (2016). 3-D elasticity buckling solution for simply supported thick rectangular plates using displacement potential functions. Applied Mathematical Modelling, 40(11–12), 5717–5730. doi:10.1016/j.apm.2015.12.034.